Original Article | Open Access

Microbiome Research Reports

Hao *et al. Microbiome Res Rep.* 2026;5:33 **DOI:**10.20517/mrr.2026.77

Engineered *Escherichia coli* expressing monoamine oxidase A modulates gut serotonin and reduces anxiety-like behaviors in mice

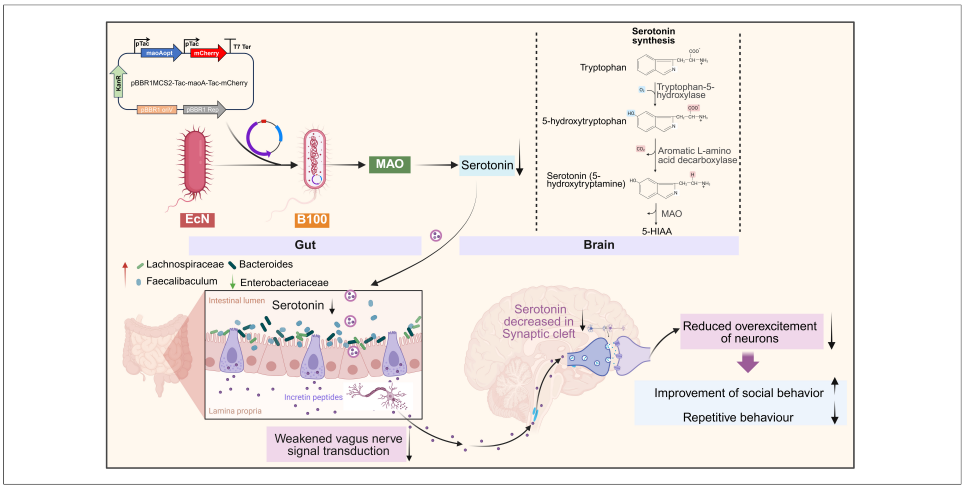
Chong Hao[1,#], Jingbai Wen[2,#], Jifeng Wang[3,4,#], Xueting Li[1], Zhaoshen Li[1], Weiliang Hou[1]

Keywords:
Autism spectrum disorder, monoamine oxidase A, gut microbiota, serotonin

Citation: Hao C, Wen J, Wang J, Li X, Li Z, Hou W. Engineered *Escherichia coli* expressing monoamine oxidase A modulates gut serotonin and reduces anxiety-like behaviors in mice. *Microbiome Res Rep.* 2026;5:33. https://dx.doi.org/10.20517/mrr.2026.77

Received: 21 Aug 2026 **First Decision:** 30 Sep 2026 **Revised:** 13 Nov 2026 **Accepted:** 19 Nov 2026 **Published:** 27 Nov 2026

Academic Editor: Rodolphe Barrangou
Copy Editor: Shu-Yuan Duan
Production Editor: Shu-Yuan Duan



Abstract

Background: Elevated peripheral serotonin levels occur in approximately 25%-30% of individuals with autism spectrum disorder (ASD). However, the causal relationship between peripheral serotonergic dysregulation and core behavioral deficits remains unclear. Novel strategies are needed to precisely modulate gut-derived serotonin and alleviate ASD-related behaviors.

Methods: Using a valproic acid (VPA)-induced mouse model of ASD, we established a preclinical intervention involving an engineered *Escherichia coli* Nissle 1917 strain (B100) that maintains functional monoamine oxidase A (MAO-A) expression. Mice received daily oral administration of B100 for four weeks. Treatment effects were assessed using behavioral tests, untargeted serum metabolomics, and fecal 16S rRNA gene sequencing to

Check for updates

[1]Department of Gastroenterology, Shanghai Institute of Pancreatic Diseases, National Key Laboratory of Immunity and Inflammation, Changhai Clinical Research Unit, Changhai Hospital, Naval Medical University, Shanghai 200433, China.
[2]School of Pharmacy, Yichun University, 576 Xuefu Road, Yichun, 336000, Jiangxi, China.
[3]Clinical Medicine Scientific and Technical Innovation Park, Shanghai Tenth People's Hospital Affiliated to Tongji University, Shanghai 200072, China.
[4]Vanderbilt University Medical Center, Nashville, TN 37232, USA.
[#]These authors contributed equally to this work.

Correspondence to: Prof. Weiliang Hou, Prof. Zhaoshen Li, Department of Gastroenterology, Shanghai Institute of Pancreatic Diseases, National Key Laboratory of Immunity and Inflammation, Changhai Clinical Research Unit, Changhai Hospital, Naval Medical University, Shanghai 200433, China. E-mail: houweiliang@tongji.edu.cn; zhsl@vip.163.com

characterize the gut microbiota.

Results: Four weeks of B100 treatment significantly improved social interaction and reduced anxiety-like behaviors compared with the VPA control group. Untargeted serum metabolomics analyses revealed that B100 treatment reduced serum tryptophan and serotonin levels, and ameliorated VPA-induced disturbances in lipid and amino acid metabolism. Furthermore, B100 treatment altered gut microbiota composition, increasing the relative abundance of beneficial taxa and reducing dysbiosis.

Conclusion: Our findings suggest that an MAO-A-expressing probiotic may alleviate ASD-related behaviors in mice through coordinated modulation of systemic metabolism and gut microbiota composition. This study presents a potential strategy for treating ASD-related behavioral abnormalities through targeted manipulation of gut microbial metabolism.

INTRODUCTION

Autism spectrum disorder (ASD) is a complex neurodevelopmental disorder characterized by impairments in social interaction and communication, as well as restricted and repetitive behaviors. It affects approximately 1 in 36 children worldwide[1,2]. The etiology of ASD is multifactorial, involving genetic, environmental, and neurobiological factors. However, effective diagnostic biomarkers and curative treatments remain lacking. Recently, the gut microbiota has emerged as a crucial modulator of ASD pathogenesis[3]. Gut microbial dysbiosis has been implicated in various neuropsychiatric disorders[4]. Notably, alterations in the gut microbiota can influence brain function and behavior through the gut-brain axis, making microbiota-targeted interventions a promising therapeutic approach for ASD[5-7].

Serotonin (5-hydroxytryptamine, 5-HT) is an essential bioactive molecule involved in regulating various physiological processes[8]. Elevated serum serotonin levels have been reported in children with ASD[9]. Over 90% of peripheral serotonin is synthesized and secreted by intestinal enterochromaffin cells, with gut microbial metabolites and intestinal homeostasis playing important roles in regulating its synthesis and metabolism[10,11]. Tryptophan (Trp), the precursor of serotonin, can be metabolized through several pathways. Serotonin synthesis occurs predominantly in the gastrointestinal tract, particularly in the colon[12]. Disruptions in tryptophan metabolism and serotonergic homeostasis have been associated with peripheral serotonergic dysregulation in ASD. Although peripheral serotonin cannot cross the blood-brain barrier, it may indirectly influence central nervous system functions through the gut-brain axis. Therefore, targeting peripheral serotonin metabolism may represent a potential therapeutic strategy for ASD[13].

Mammalian monoamine oxidase (MAO) comprises two isoforms, MAO-A and MAO-B. MAO-A has a high substrate affinity for serotonin and plays a key role in its oxidative deamination and degradation[14,15]. In this study, we engineered a recombinant probiotic strain to maintain functional MAO-A expression, aiming to modulate gut-derived serotonin metabolism and improve ASD-related behavioral abnormalities. Specifically, we synthesized and optimized the codon sequence of the mouse MAO-A gene for expression in *Escherichia coli* Nissle 1917 (EcN). The recombinant gene was cloned into an expression plasmid and introduced into EcN by electroporation, generating the engineered strain B100, which expressed functional MAO-A. We further tested the effects of B100 administration on ASD-related behaviors, gut microbiota composition, and serum metabolite profiles in a valproic acid (VPA)-induced mouse model of ASD. Our results demonstrated that B100 treatment alleviated ASD-related behavioral abnormalities, altered gut microbiota composition, and ameliorated metabolic disturbances in mice. These findings support the potential of engineered probiotics to modulate gut microbial metabolism and provide a foundation for further mechanistic exploration and translational research.

MATERIALS AND METHODS

Strains and culture conditions

The EcN was used as the host strain for plasmid construction. EcN carrying pBBR1MCS2-Tac-maoA-Tac-mCherry (strain B100) was also provided by Sangon Biotech Co. (Shanghai, China). The empty-plasmid control strain was EcN transformed with pBBR1MCS2-Tac-mCherry. All strains were cultured in Luria-Bertani (LB) medium at 37 °C and 200 rpm, unless otherwise specified. The B100 strain was cultured in LB medium supplemented with 50 μg/mL of kanamycin to maintain selection for the plasmid. The B100 and EcN were cultured and subjected to serial passages prior to experiments.

Enzymes and reagents

The DNA polymerase and the seamless cloning kit were purchased from Vazyme Biotech Co., Ltd. (Nanjing, China). The CheKine™ Micro Monoamine Oxidase (MAO) Activity Assay Kit was purchased from Abbkine. Kanamycin was purchased from Shanghai Titan Scientific Co., Ltd.

Animals and housing

All animal experiments were approved by the Institutional Animal Care and Use Committee of Shanghai Tenth People's Hospital (approvalnumber: SHDSYY-2021- 4977). C57BL/6J wild-type (WT) mice were obtained from Shanghai Bikai Laboratory Animal Technology Co., Ltd. A total of 14 pregnant dams were used in this study. To minimize litter bias, male offspring from each litter were distributed across different experimental groups. To avoid potential confounding by the estrous cycle, only male mice were used in the behavioral assays. Mice were housed in a specific pathogen-free animal facility under a 12-h light/12-h dark cycle, with controlled temperature (22 ± 2 °C) and humidity (50% ± 10%). Randomization was performed using a random number generator after weaning. Behavioral testing and raw data analysis were conducted by researchers blinded to group assignments, while the investigator performing oral gavage was not blinded. Predefined exclusion criteria included severe illness, injury, death, or recording equipment failure. No animals were excluded from the final analysis. Group sizes were determined based on previous studies using the VPA model and our preliminary data to achieve adequate statistical power.

Plasmid and recombinant strain construction

The MAO-A coding sequence of Mus musculus was first retrieved from the NCBI (Gene ID: 17161) and subjected to codon optimization based on the codon usage of EcN. The obtained sequence was then synthesized by Shanghai Personalbio Technology Co., Ltd. (Shanghai, China). The maoA gene was amplified from the synthesized maoA gene product using primers Tac-maoA-F (5'-caggtttcccgactgttgacaattaatcatcggctcgtataatgaattccaaggatatataccatgaccgatctggaaaaaccg-3') and maoA-R (5'-gggagagcgtcgagatcccggagctcgaattcttaactctgaggctgcttaaatt-3'). The pBBR1MCS2-Tac-maoA-Tac-mCherry plasmid was first linearized by polymerase chain reaction (PCR) using the primers pBBR1-VF (5'-cgggatctcgacgctctccct-3') and pBBR1-VR (5'-cagtcgggaaacctgtcgtgc-3'). The primer was designed to introduce the constitutive Tac promoter upstream of the maoA gene. These two amplified products were then purified and assembled together by the seamless cloning kit, resulting in the maoA co-expressing plasmid pBBR1MCS2-Tac-maoA-Tac-mCherry, as shown in Figure 1A. The constructed plasmid was confirmed by DNA sequencing and then electroporated into EcN cells as described previously[16], thereby generating strain B100.

Protein sample preparation and sodium dodecyl sulfate-polyacrylamide gel electrophoresis (SDS-PAGE) analysis

The EcN (empty plasmid) and B100 (MAO-A expression plasmid) strains were cultured overnight in 5 mL LK medium (LB medium containing 50 μg/mL kanamycin) at 37 °C with shaking at 200 rpm. Then the cells were inoculated at a 1% (v/v) ratio into 20 mL LK medium, and incubated under identical conditions for 48

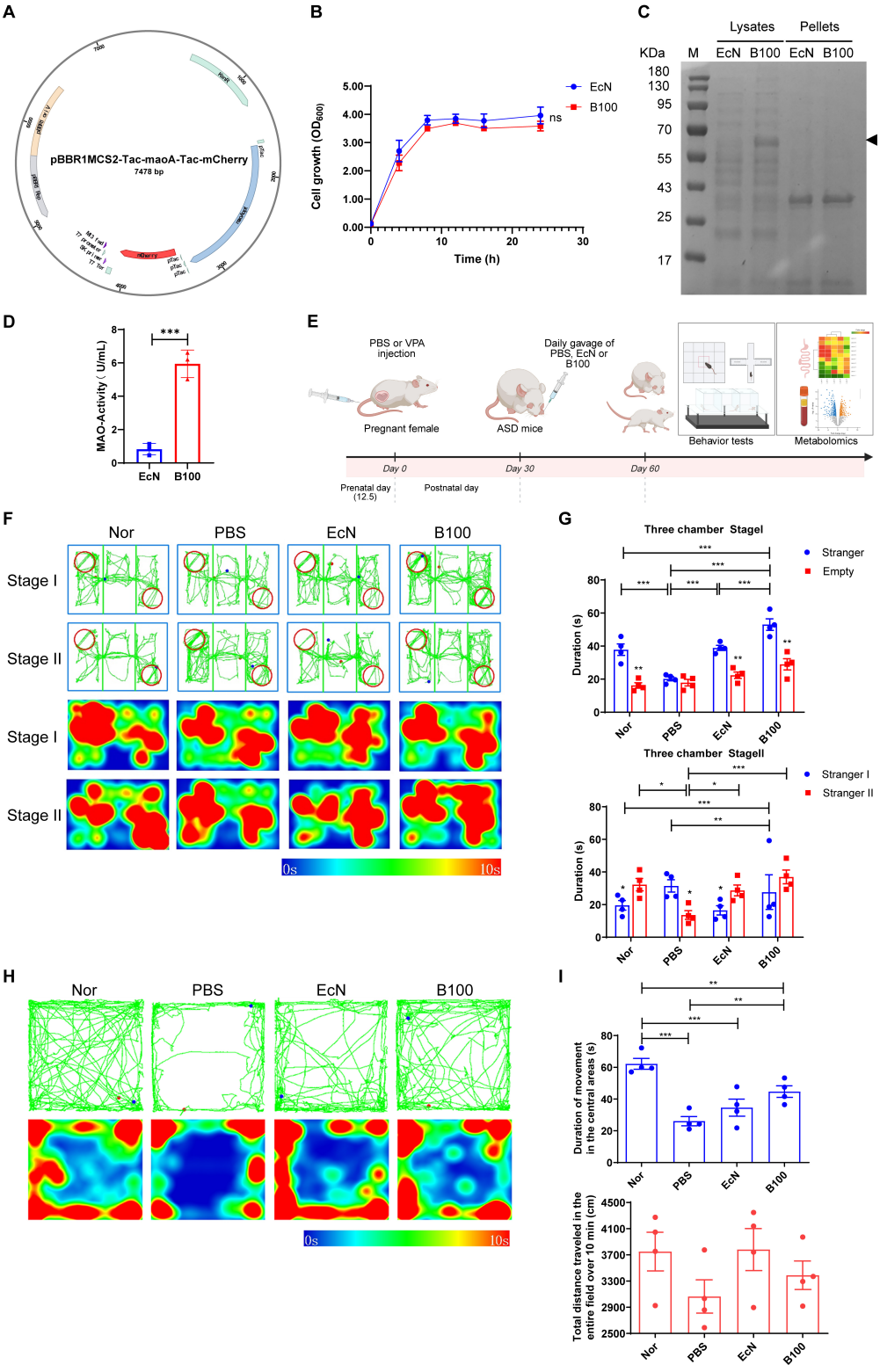


Figure 1. Identification of recombinant strains and alleviation of ASD-related behaviors in a VPA mouse model. (A) Schematic representation of plasmid pBBR1MCS2-Tac-maoA-Tac-mCherry; (B) Effect of plasmid introduction on the growth of EcN and B100; (C) SDS-PAGE analysis of MAO-A expression. M denotes the molecular-weight marker; lanes 1 and 3 show the soluble lysate and insoluble pellet fractions of EcN, respectively; lanes 2 and 4 show the corresponding fractions of B100; (D) MAO-A activity in EcN and B100; (E) Schematic of the experimental design and timeline for establishing the prenatal VPA model. After the offspring were obtained, male offspring of saline-treated dams (Normal) and of VPA-treated dams (VPA + PBS, VPA + EcN, VPA + B100) received the corresponding treatment by daily gavage for 4 weeks (n = 4 per group) Create with BioRender; (F) Representative movement trajectories and heat maps from the three-chamber social interaction test; (G) Time spent in the empty and stranger I areas during stage I, and in the stranger II and stranger I areas during stage II; (H) Representative heat maps showing time spent in each area of the open field chamber; (I) Time spent in the central zone and total distance traveled during the 10-min test. All values are expressed as mean ± SEM. *P < 0.05, **P < 0.01, ***P < 0.001. OD_{600}: Optical density at 600 nm; EcN: *Escherichia coli* Nissle 1917; PBS: phosphate-buffered saline; MAO-A: maintains functional

monoamine oxidase A; VPA: valproic acid; B100: engineered *Escherichia coli* Nissle 1917 strain; ASD: autism spectrum disorder; SDS-PAGE: sodium dodecyl sulfate-polyacrylamide gel electrophoresis; Nor: normal control group; SEM: standard error of the mean.

h. Bacterial pellets were collected by centrifugation at 12,000 rpm for 5 min at 4 °C. The cell pellets were washed with ice-cold phosphate-buffered saline (PBS) and resuspended in an equal volume of PBS, and then sonicated for 5 min at 200 W using 5-s pulses separated by 5-s intervals. Then the samples were centrifuged at 12,000 rpm for 30 min at 4 °C and the supernatants were used as the soluble intracellular protein samples. The pellets were then washed three times, resuspended in an equal volume of ice-cold PBS, and used as the insoluble protein samples. Appropriate volumes of the protein samples were combined with loading buffer and heated in a boiling-water bath for 3 min. Once cooled to room temperature, the mixtures were centrifuged at 12,000 rpm for 5 min, and 10 μL aliquots were loaded onto the gel for SDS-PAGE.

MAO-A activity determination

The MAO-A activity of the recombinant cells was determined by the CheKine™ Micro Monoamine Oxidase (MAO) Activity Assay Kit (Cat #: KTB1900). Sample preparation and activity measurements were performed according to the kit manufacturer's instructions. One unit of MAO-A activity was defined as the amount of enzyme activity that converts 1 nmol of substrate per minute at 37 °C and pH 7.6 in 1 mL of cells at an OD600 of 1.

VPA-induced ASD mouse model

The prenatal VPA-induced mouse model of ASD was established following a published protocol[17]. Briefly, pregnant wild-type female mice received a single intraperitoneal injection of 500 mg/kg VPA (Sigma-Aldrich, St. Louis, MO, USA), while control dams were administered an equivalent volume of 0.9% PBS as the vehicle on embryonic day 12.5 (E12.5). A total of 14 pregnant dams (4 PBS-treated and 10 VPA-exposed dams) were used in this study. Normal group: 4 litters, with 1 male pup contributed by each litter; VPA + PBS group: 4 litters, with 1 male pup contributed by each litter; VPA + EcN group: 4 litters, with 1 male pup contributed by each litter; VPA + B100 group: 4 litters, with 1 male pup contributed by each litter. Among the 10 VPA dams, 8 dams provided offspring to only one VPA group, while 2 dams contributed male pups to two distinct VPA groups. To minimize litter bias, at most one male pup from a given litter was allocated to the same group, and a maximum of two male pups from one litter were distributed across different groups. Each group contained 4 male mice. After weaning, male offspring were randomly assigned to four experimental groups (n = 4 per group): (1) Normal group, male offspring of saline-treated dams, receiving 100 μL sterile PBS daily by gavage; (2) VPA + PBS group, male offspring of VPA-treated dams, receiving 100 μL PBS daily by gavage; (3) VPA + EcN group, male offspring of VPA-exposed dams, receiving 100 μL EcN bacterial [10^9 colony-forming units (CFU)] suspension daily by gavage; (4) VPA + B100 group, male offspring of VPA-exposed dams, receiving 100 μL B100 bacterial (10^9 CFU) suspension daily by gavage. All gavage treatments were initiated at 1 month of age and administered once daily for 4 consecutive weeks. Behavioral phenotyping was performed when the animals reached 2 months of age. Body weight of each mouse was recorded individually every 3-4 days throughout the intervention period. Measurements were performed at a fixed time of day to reduce variation. After behavioral assays, fecal samples were collected from these identical animals for 16S rRNA sequencing.

Behavioral studies

Following a 4-week intervention period, the mice were subjected to social interaction and open-field tests. On the day of testing, they were housed in sterile filtered cages and acclimated for an hour in an adjacent room before the tests. Between individual animal tests, the testing arena was sequentially wiped with disinfectant, 70% ethanol, and distilled water.

The three-chamber social interaction test

The three-chamber social interaction test was performed as previously described[18]. The three-chamber apparatus comprises three compartments of identical dimensions (20 cm × 45 cm each), divided by transparent plexiglass panels with connecting openings. The animals used in the experiment were paired with unfamiliar mice of the same sex and strain. At the start of the experiment, the subject mouse was placed in the central chamber, while the unfamiliar mouse was confined in a wire cage in one chamber and an empty wire cage was placed in the other chamber. Following a 5-min habituation phase, social interaction was recorded over a 10-min period. During the social novelty preference test, a novel mouse was placed in the wire cage of the alternate chamber. The subject mouse was placed back in the central chamber and permitted to explore all three chambers freely for another 10 min, with its movements continuously recorded.

Open-field test

The open-field test was performed as described previously[19], in a white Plexiglas arena measuring 50 cm × 50 cm. The floor was virtually divided into nine equal zones to record locomotor activity over a 10-min period. Each mouse was carefully placed at the arena center for behavioral recording. We quantified three main readouts throughout the test: time spent in the central zone, total distance traveled, and mean movement speed. Longer central residence time or shorter latency to access the central zone reflects reduced anxiety-like behavior, whereas the opposite pattern indicates elevated anxiety.

Mouse stool collection and 16S sequencing

Fresh fecal pellets were harvested at euthanasia and snap-frozen promptly for subsequent DNA extraction and 16S rRNA gene sequencing. Fecal genomic DNA was isolated with HiPure stool DNA kits (Magen, Guangzhou, China) following the manufacturer's protocols. Barcoded primers targeting the V4 hypervariable region (515F/806R) were used for PCR amplification of the 16S rRNA gene[20]. DNA library sequencing was carried out on an Illumina NovaSeq 6000 platform in PE250 mode at Gene Denovo Biotechnology Co., Ltd (Guangzhou, China). Quality-filtered reads were binned into operational taxonomic units (OTUs) at 97% sequence similarity via the UPARSE pipeline (v9.2.64)[21]. UCHIME was applied to identify and remove chimeric sequences. The high-quality, chimera-free reads were used for OTU abundance profiling and subsequent analyses, and the most prevalent sequence of each OTU was selected as the representative sequence.

Untargeted metabolomic profiling of serum samples

Untargeted metabolomic profiling of serum samples was conducted by Gideon Biotechnology Co., Ltd. (Guangzhou, China) using gas chromatography-mass spectrometry (GC-MS) and liquid chromatography-mass spectrometry (LC-MS). Briefly, serum samples (50 μL) collected from mice were subjected to methanol extraction, followed by lyophilization for GC-MS metabolomic profiling. Next, methoxylamine hydrochloride (15 mg/mL in pyridine) was combined with the residues, and the mixture was incubated at 37 °C for 60 min. Bis (trimethylsilyl) trifluoroacetamide (BSTFA, containing 1% trimethylchlorosilane) and n-hexane were added. The derivatization reaction was carried out at 70 °C for 60 min, and samples were then equilibrated at ambient temperature for 30 min prior to detection. Prepared derivatives were separated and measured with an Agilent 8890-5977B GC-MS system fitted with a DB-5MS column. For LC-MS analysis, serum metabolites were extracted by precipitation with ice-cold acetonitrile. Chromatographic separation was performed on a BEH C18 column using a water-acetonitrile gradient containing 0.1% formic acid. Mass spectra were acquired in positive- and negative-ion electrospray ionization (ESI) modes using a quadrupole time-of-flight (Q-TOF) mass spectrometer over an m/z range of 50-1,200. Quality-control (QC) pooled samples were injected to assess system stability. Raw data were processed for peak alignment and metabolite identification.

Serum serotonin measurement

Under isoflurane anesthesia, mouse blood was harvested from the retro-orbital venous plexus with plain glass capillaries in line with standard animal sampling protocols. Whole blood samples were maintained at room temperature for 30 min and then centrifuged at 1,000 ×*g* for 10 min at 4 °C. The upper serum fraction was gently transferred to new tubes and preserved at -20 °C pending subsequent assays. Serum serotonin concentrations were quantified with a commercial enzyme-linked immunosorbent assay (ELISA) kit (Eagle Biosciences, USA) as specified in the manufacturer's manual. All animal manipulations complied with institutional guidelines for animal welfare and experimentation.

Statistical analysis

All omics datasets in this work were processed via the open Oebiotech Cloud Platform (https://cloud.oebiotech.cn/task/). Behavioral data were analyzed using repeated-measures one-way analysis of variance (ANOVA) followed by Bonferroni-Dunnpost-hoccomparisons. A two-tailed Student's *t*-test was used to assess differences between groups in metabolite levels. For gut microbial α-diversity, one-way ANOVA followed by Tukey's honestly significant difference (HSD) test was used for comparisons among groups. For relative abundance of bacterial taxa, one-way ANOVA followed by Tukey's HSD post-hoc test was performed. Differential metabolites were screened using thresholds of variable importance in projection (VIP) > 1.5 and $P < 0.05$. Differential bacterial taxa were identified using the Benjamini-Hochberg procedure to control the false discovery rate (FDR), and an adjusted *P*-value < 0.05 was set as the significance threshold. The Benjamini-Hochberg FDR correction across all pairwise comparisons was applied to all tested microbial features for multiple testing adjustment. All results are expressed as mean ± standard error of the mean (SEM), and statistical significance was defined as $P < 0.05$. Statistical Package for the Social Sciences (SPSS) software (version 22.0, IBM, Armonk, NY, USA) was used for statistical analyses. GraphPad Prism 9.0, Adobe Illustrator 2024 and BioRender were utilized for figure generation.

RESULTS

Construction and functional validation of an MAO-A-expressing engineered strain

The recombinant plasmid pBBR1MCS2-Tac-maoA-Tac-mCherry was successfully constructed and introduced into EcN, generating the engineered strain B100 [Figure 1A]. Growth curve analysis confirmed that plasmid introduction did not noticeably affect bacterial proliferation, as B100 exhibited a growth profile comparable to that of the EcN strain [Figure 1B]. SDS-PAGE analysis revealed a distinct band between 55 and 70 kDa in the soluble intracellular protein fraction of B100 (lane 2), whereas no corresponding band was detected in the control EcN strain (lane 1, Figure 1C). The estimated molecular weight of this band matched that of MAO-A (59.6 kDa), supporting successful MAO-A expression in EcN cells. Furthermore, enzymatic activity assays revealed that the B100 strain displayed markedly higher MAO-A activity (5.81 ± 1.13 U/mL) than the control EcN strain (0.80 ± 0.48 U/mL; Figure 1D). Collectively, these results confirmed the successful expression of a functional MAO-A enzyme in the engineered B100 strain.

Engineered strain B100 alleviates ASD-related behaviors in a VPA-induced mouse model

To investigate the effects of B100 on ASD, we constructed a VPA-induced mouse model [Figure 1E]. Behavioral tests were performed to characterize VPA-induced abnormalities. In the first phase of the three-chamber sociability test, mice in the normal control group (Nor) interacted with a stranger mouse for a significantly longer duration than with an empty cup, demonstrating the expected social preference [Figure 1F and G]. In contrast, VPA-treated mice receiving PBS showed no preference for the stranger mouse over the empty cup, suggesting a lack of sociability. EcN treatment restored this social preference, while B100 treatment produced a more pronounced improvement. In the second phase, which assessed social novelty preference, mice in the normal control group preferred a novel mouse over a familiar mouse, whereas the VPA-treated mice receiving PBS exhibited the opposite preference, favoring the familiar mouse. Similarly,

EcN supplementation restored the preference for social novelty. In contrast, B100-treated mice exhibited comparable exploration of novel and familiar mice, indicating that B100 attenuated the preference for the familiar mouse observed in VPA-treated controls. This finding suggests that B100 may modify social novelty-related behavior, although the lack of a clear preference for the novel mouse does not establish a complete restoration of normal social novelty preference. Body weight was monitored routinely during intervention, and no obvious growth retardation was noted across groups.

In the open field test, VPA-treated mice receiving PBS displayed anxiety-like behavior, characterized by reduced exploration of the central zone. B100 treatment markedly increased the time spent in the central zone compared with the PBS group (PBS *vs.* B100, $P = 0.0011$), while EcN treatment did not produce significant anxiolytic effects [Figure 1H and I]. Overall, these findings indicate that B100 treatment ameliorated certain ASD-related behavioral abnormalities in VPA-exposed mice, including impaired sociability and anxiety-like behaviors.

Effects of recombinant strains on intestinal microbiota

Given the observed behavioral improvements, we further examined whether EcN or B100 administration altered gut microbiota composition. 16S rRNA gene sequencing of 16 fecal samples revealed that α-diversity (Shannon and Simpson indices) was comparable across all groups [Figure 2A]. In contrast, β-diversity analyses [principal coordinates analysis (PCoA) and partial least squares discriminant analysis (PLS-DA)] demonstrated distinct clustering patterns among the treatment groups [Figure 2B and C]. Venn and UpSet intersection analyses across the four groups (PBS, Nor, EcN, B100) revealed 62 shared genera and 28 shared species [Figure 2D and E]. Unweighted pair group method with arithmetic mean (UPGMA) clustering analysis revealed two primary clusters at the order level. The Normal group clustered closely with either the B100 or EcN group, whereas the PBS group formed a separate branch [Figure 2F].

At the class level, VPA exposure was associated with a decreased relative abundance of *Bacteroidia* and an increased relative abundance of *Clostridia*. At the order level, the relative abundances of *Bacteroidales* and *Lachnospirales* decreased, while that of *Clostridia*_UCG-014 increased. EcN and B100 treatments reversed these changes [Figure 2G]. Ternary plots further illustrated the distribution of microbial taxa across the treatment groups at the family, genus, and species levels [Figure 2H]. Additionally, linear discriminant analysis effect size (LEfSe) identified differentially abundant taxa at the family level [linear discriminant analysis (LDA) > 2], as summarized in the cladogram [Figure 2I]. Compared with the EcN group, the B100 group exhibited a significantly lower relative abundance of *Enterobacteriaceae*, a bacterial family reported to be enriched in some individuals with ASD. In contrast, B100 treatment increased the relative abundance of *Faecalibaculum* and its species *Faecalibaculum rodentium*, which have been linked to beneficial metabolic functions, including short-chain fatty acid production [Figure 2J]. Because *Enterobacteriaceae* is a Gram-negative bacterial family, its reduced abundance may indicate a potential decrease in lipopolysaccharide (LPS)-related inflammatory burden. Similarly, enrichment of potentially beneficial bacteria may contribute to intestinal barrier maintenance and immune homeostasis. However, these proposed effects require further investigation because serum LPS and inflammatory cytokine data were not directly measured.

Circos diagrams were also used to visualize the distribution of dominant species across samples [Figure 3A and B]. Microbial phenotypic and functional profiles were further predicted using BugBase, functional annotation of prokaryotic taxa (FAPROTAX), and Tax4Fun [Figure 3C-F]. BugBase analysis showed that VPA exposure enriched potentially pathogenic, facultatively anaerobic and biofilm-forming microbes, whereas B100 treatment reduced potentially pathogenic bacteria [Figure 3C and D]. Consistent with phenotypic changes, FAPROTAX functional analysis demonstrated that chemoheterotrophy and fermentation dominated the core microbial functions in the PBS group. B100 intervention reshaped the

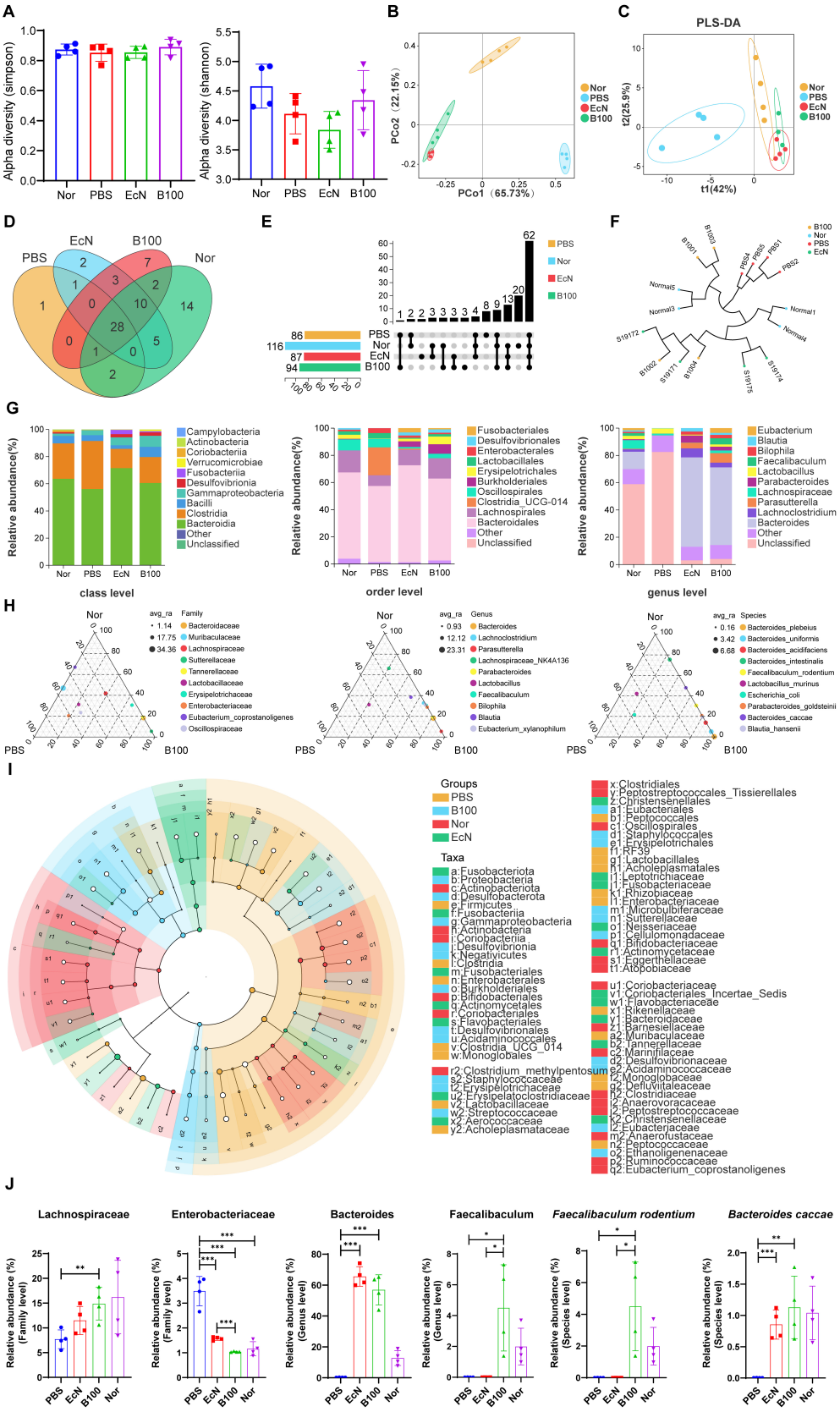


Figure 2. Recombinant strain reshaped gut microbiota composition. (A) Shannon and Simpson α-diversity indices; (B) β-diversity assessed using weighted PCoA; (C) β-diversity visualized using PLS-DA score plots; (D) Venn diagram showing the overlap among the four groups at the species level; (E) UpSet plot showing the overlap among the four groups at the genus level; (F) Dendrogram derived from UPGMA cluster analysis, showing the relationships between the four groups; (G) Relative abundance of the 12 most abundant taxa at the class, order, and genus levels; (H) Ternary plots showing the composition and relative distribution of microbiota at the family, genus, and species levels; (I) Cladogram from the LEfSe analysis at the family level (LDA > 2); (J) Dominant and differentially abundant taxa at the family, genus, and species levels. Data are presented as mean ± SEM (n = 4). For alpha diversity indices, one-way ANOVA followed by Tukey's

HSD post-hoc test was used for multi-group comparison. For relative abundance of bacterial taxa, one-way ANOVA followed by Tukey's HSD post-hoc test was performed. Differential taxa were identified with Benjamini-Hochberg FDR correction for multiple testing across all microbial features; an adjusted *P*-value < 0.05 was defined as statistically significant. **P* < 0.05, ***P* < 0.01, ****P* < 0.001. PBS: Phosphate-buffered saline; EcN: *Escherichia coli* Nissle 1917; Nor: normal control group; B100: engineered *Escherichia coli* Nissle 1917 strain; PCoA: principal coordinates analysis; PLS-DA: partial least squares discriminant analysis; UPGMA: unweighted pair group method with arithmetic mean; LEfSe: linear discriminant analysis effect size; LDA: linear discriminant analysis; SEM: standard error of the mean; ANOVA: analysis of variance; HSD: honestly significant difference; FDR: false discovery rate.

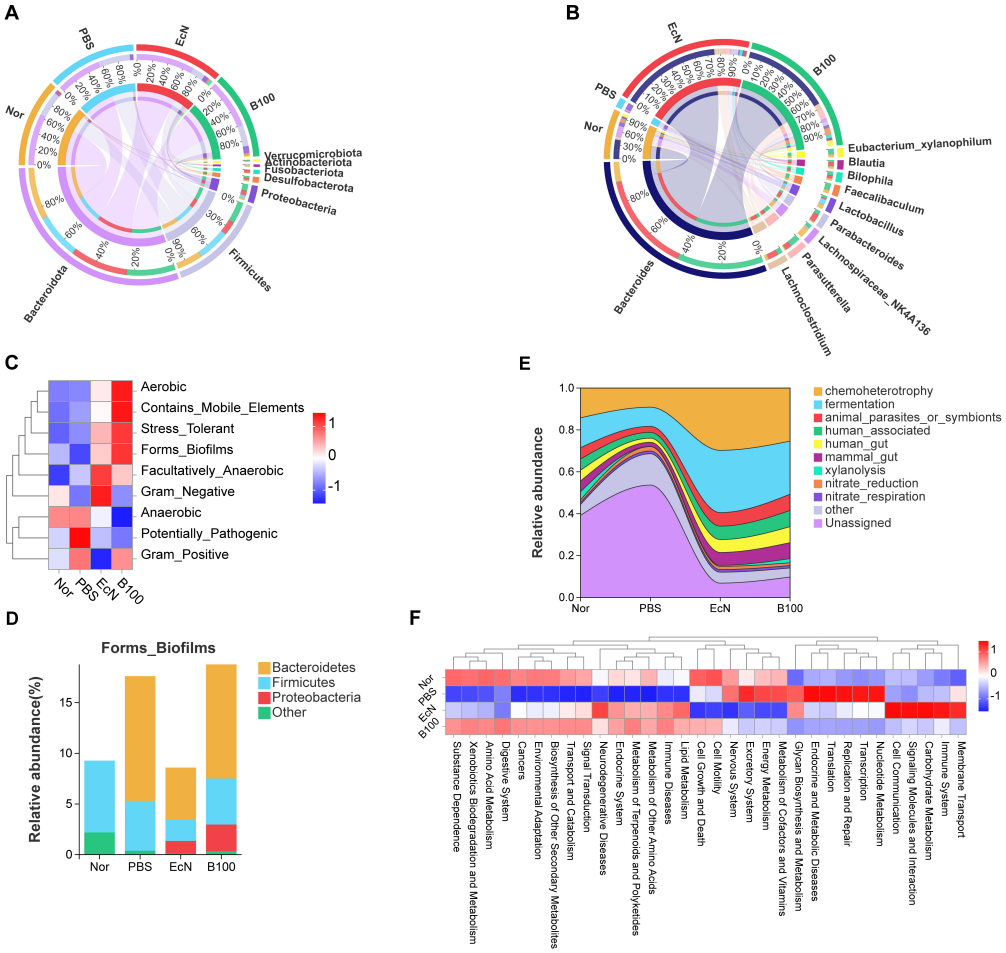


Figure 3. Functional prediction of gut microbiota following recombinant strain intervention. (A) Circos diagram showing taxa at the phylum level; (B) Circos diagram showing taxa at the genus level; (C) BugBase was used to predict microbial phenotypes; (D) Biofilm-forming potential across the different groups. The functional profiles of the bacterial communities and their ecological functions were explored using FAPROTAX (E) and Tax4Fun (F). PBS: Phosphate-buffered saline; EcN: *Escherichia coli* Nissle 1917; Nor: normal control group; B100: engineered *Escherichia coli* Nissle 1917 strain; FAPROTAX: functional annotation of prokaryotic taxa.

functional structure of the gut microbiota, with a reduction in the proportion of unassigned functions and altered metabolic capacity for nitrogen cycling [Figure 3E]. Tax4Fun-based functional prediction further indicated pervasive alterations in microbial metabolic pathways. The VPA challenge perturbed pathways including amino acid metabolism, lipid metabolism, and signal transduction. B100 treatment largely restored these dysregulated metabolic and signaling functions towards the status observed in the normal control group [Figure 3F]. Collectively, these results suggest that B100 treatment altered VPA-associated gut microbial dysbiosis, shifting the microbial community composition and function toward that observed in the Normal group.

Recombinant strain B100 ameliorated VPA-induced serum metabolic disturbances

To characterize probiotic-induced metabolic alterations, we performed untargeted serum metabolomics across normal, PBS, EcN, and B100 groups. Representative total ion chromatograms (TICs) are depicted in Figure 4A. Orthogonal partial least squares discriminant analysis (OPLS-DA) demonstrated clear metabolic separation between PBS and B100 groups, and between EcN and B100 groups, indicating that B100 treatment was associated with changes in serum metabolism [Figure 4B]. Permutation tests (200 iterations) validated the reliability and robustness of OPLS-DA models [Figure 4C]. Under the screening criteria of VIP > 1.5 and $P < 0.05$, 213 differential metabolites were identified between B100 and PBS groups [Figure 4D]. The samples from the two groups were well separated, indicating a profound shift in metabolic profiles upon B100 treatment. Multiple long-chain fatty acids, including oleic acid, linoleic acid, palmitic acid and palmitelaidic acid, were enriched in PBS-treated mice and markedly reduced after B100 administration. Consistently, volcano plots and KEGG (Kyoto Encyclopedia of Genes and Genomes) enrichment analysis showed that B100 remodeled lipid metabolism [Figure 4E-G].

Similarly, we further compared the metabolic profiles between the EcN and B100 groups. Metabolic pathway enrichment analysis identified 12 differentially abundant metabolites after B100 intervention, including 4 upregulated and 8 downregulated metabolites, thereby revealing significant alterations in tryptophan metabolism [Figure 5A]. Consistently, volcano plots illustrated widespread metabolite changes after B100 treatment, predominantly associated with lipid and amino acid metabolism pathways [Figure 5B and C]. Specifically, VPA exposure significantly increased serum palmitic acid and oleic acid levels, which were significantly reduced after B100 administration. Regarding tryptophan metabolism, serum L-tryptophan levels were decreased in the B100 group compared with the EcN group [Figure 5D]. Additionally, serum serotonin concentration was significantly elevated in VPA + PBS group mice, while B100 treatment effectively reduced peripheral serotonin levels [Figure 5E]. Correlation analysis further revealed strong interrelationships among differential metabolites, reflecting coordinated systemic metabolic changes induced by B100 intervention [Figure 5F]. Notably, the metabolic alterations observed in the present study are correlational findings. Although B100 expresses functional MAO-A and regulates peripheral tryptophan and serotonin levels, the current data cannot fully exclude alternative regulatory pathways. Collectively, our metabolomics results indicate that B100 intervention profoundly reverses VPA-induced disturbances in lipid and amino acid metabolism, restores peripheral metabolic homeostasis, and is accompanied by reduced serum tryptophan and serotonin levels in ASD model mice [Figure 5G].

DISCUSSION

In this study, we explored the potential therapeutic effects of an engineered EcN strain expressing MAO-A in a VPA-induced ASD mouse model. Our results demonstrated that oral delivery of B100 altered gut microbiota and host metabolic profiles in VPA-exposed mice, thus significantly alleviating core ASD-related behaviors, including social deficits and anxiety-like behaviors. Mechanistically, B100 treatment reshaped the gut microbiota composition and ameliorated metabolic disturbances, particularly in lipid and amino acid metabolism. We propose that the remodeling of gut microbial homeostasis and systemic metabolic reprogramming are associated with the behavioral improvements observed in model mice. Collectively, our results support the concept that precisely engineered probiotics can exert systemic therapeutic effects by integrating enzymatic activity, microbial remodeling, and metabolic reprogramming.

In the social novelty preference test, B100-treated mice did not show the same preference for the novel mouse as the controls; however, treatment eliminated the familiar-mouse preference in VPA-exposed mice. This transition from a pathologically biased social choice to a balanced exploratory pattern suggests that MAO-A-expressing probiotics counteract the social withdrawal phenotypes typical of ASD, possibly by mitigating anxiety-like states. However, we observed comparable effects in the EcN and B100 groups for

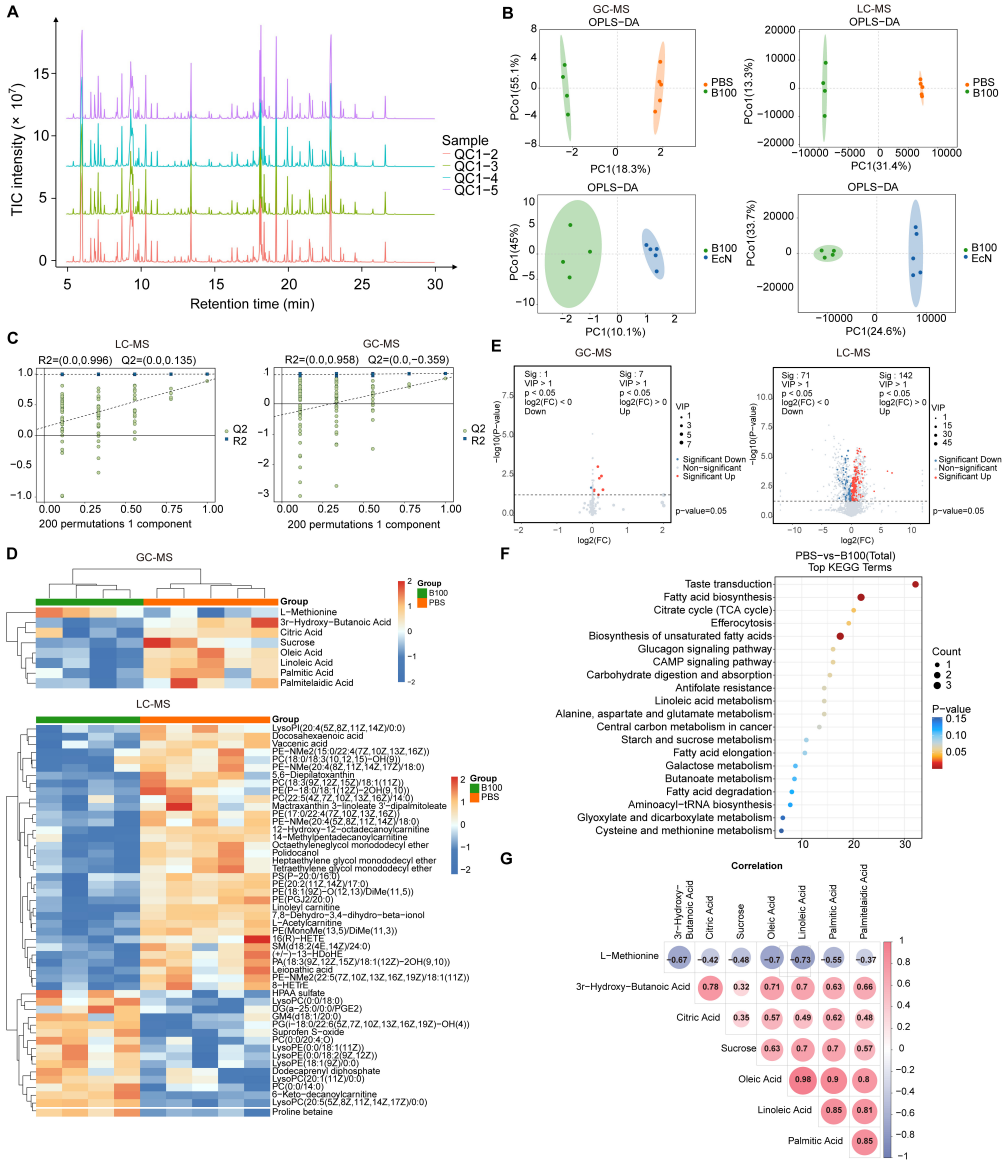


Figure 4. Serum metabolomic profiling revealed B100-induced metabolic reprogramming. (A) Overlay of TICs from the samples; (B) OPLS-DA models based on GC-MS and LC-MS data for the PBS-versus-B100 and B100-versus-EcN comparisons; (C) Permutation tests of the OPLS-DA models based on GC-MS and LC-MS data for the PBS-versus-B100 comparison; (D) Heatmap of differentially abundant metabolites in the B100 and PBS groups based on GC-MS and LC-MS data; (E) Volcano plots of the differentially abundant metabolites in the B100 group compared with the PBS control group, based on GC-MS and LC-MS data; (F) KEGG pathway enrichment analysis of significant differentially abundant metabolites in the PBS and B100 groups; (G) Correlation analysis of differentially abundant metabolites in the PBS and B100 groups. LC-MS: Liquid chromatography-mass spectrometry; OPLS-DA: orthogonal partial least squares discriminant analysis; PBS: phosphate-buffered saline; EcN: *Escherichia coli* Nissle 1917; Nor: normal control group; B100: engineered *Escherichia coli* Nissle 1917 strain; GC-MS: gas chromatography-mass spectrometry; VIP: variable importance in projection; FC: fold change; TCA: tricarboxylic acid; tRNA: transfer RNA; TIC: total ion chromatogram.

several indicators, suggesting that the parental EcN strain may partially contribute to the protective effects. Therefore, we cannot fully separate the effects of EcN and MAO-A activity in the current study. Direct oral administration of free MAO-A protein is unfeasible because gastrointestinal proteolysis rapidly abolishes enzyme activity. Future work will use an EcN strain expressing a catalytically inactive MAO-A mutant to precisely define the specific role of MAO-A.

Serotonergic dysregulation is well recognized as a crucial pathological feature of ASD and may play an important mediating role in the gut-brain-microbiome axis[9]. Targeting central serotonergic signaling

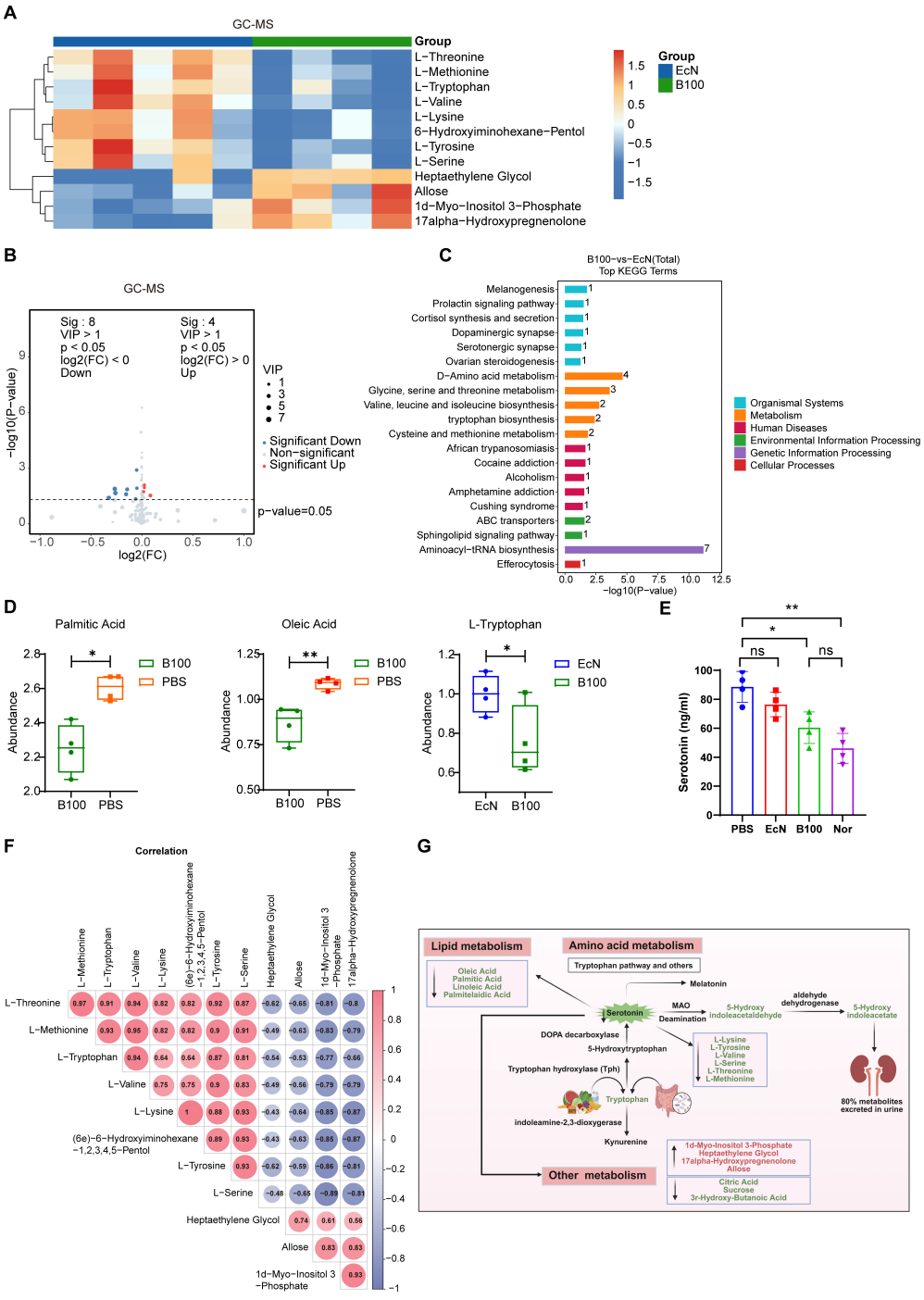


Figure 5. Serum metabolomic profiling revealed B100-induced serotonin pathway modulation. (A) Heatmap of differentially abundant metabolites in the B100 and EcN groups based on GC-MS data; (B) Volcano plot of differentially abundant metabolites comparing the B100 and EcN groups; (C) KEGG pathway classification of metabolites identified in the B100 and EcN groups; (D) Concentrations of metabolites in the B100 group compared with those in the PBS or EcN groups, as indicated; (E) Serum serotonin levels measured by ELISA; (F) Correlation analysis of differentially abundant metabolites in the EcN and B100 groups; (G) Schematic representation of serotonin metabolism. Created with BioRender. All values are expressed as mean ± SEM. *$P < 0.05$, **$P < 0.01$. GC-MS: Gas chromatography-mass spectrometry; VIP: variable importance in projection; FC: fold change; PBS: phosphate-buffered saline; EcN: *Escherichia coli* Nissle 1917; Nor: normal control group; B100: engineered *Escherichia coli* Nissle 1917 strain; ABC: ATP-bindingcassette; tRNA: transfer RNA; KEGG: Kyoto Encyclopedia of Genes and Genomes; DOPA: Dihydroxyphenylalanine; MAO: maintains functional monoamine oxidase; ELISA: enzyme-linked immunosorbent assay; SEM: standard error of the mean.

remains challenging due to the risk of off-target effects and limited therapeutic efficacy. Engineered probiotics offer a precision gut-targeted intervention strategy and can locally regulate intestinal monoamine

metabolism and circumvent the limitations of conventional approaches to central nervous system drug delivery[6]. In this work, we constructed a recombinant EcN strain that maintains functional MAO-A expression throughout the serial passages performed in this study; MAO-A is the primary enzyme responsible for the oxidative degradation of serotonin. SDS-PAGE and enzymatic activity assays confirmed the successful expression and bioactivity of MAO-A in B100. Additionally, the similar growth profiles of B100 and EcN indicated that heterologous MAO-A expression did not impose an obvious metabolic burden on the probiotic strain, supporting its potential feasibility for subsequent translational research[22].

Mounting evidence has confirmed that gut microbiota dysbiosis is tightly associated with neurobehavioral disorders through the gut-brain axis. Consistent with previous reports, VPA exposure triggered significant gut microbial disturbance in mice, characterized by a reduced abundance of *Bacteroidia* and an increased abundance of *Clostridia*, together with reduced abundances of *Lachnospiraceae* and *Bacteroides*. B100 treatment effectively reversed these compositional changes and shifted the gut microbiota composition toward that of the normal group. Enrichment of *Lachnospiraceae* may contribute to neuroprotective effects by maintaining intestinal barrier integrity and mitigating peripheral neuroinflammation[23]. Beyond microbial remodeling, untargeted metabolomic analysis further demonstrated that B100 intervention substantially ameliorated VPA-induced systemic metabolic disturbances, particularly in lipid metabolism and tryptophan-related amino acid metabolism. The reduced serum tryptophan and serotonin levels in B100-treated mice indicate altered peripheral serotonergic metabolism, which may partially account for the improved behavioral phenotypes.

Additionally, the alterations in gut microbial community composition, including the enrichment of butyrate-producing *Faecalibaculum* after B100 treatment, may arise from multiple interrelated mechanisms supported by our combined microbiota and metabolomic data. First, B100-derived MAO-A remodels gut luminal monoamine metabolism and lowers circulating tryptophan and serotonin. These metabolites serve as signals in the gut environment that regulate commensal anaerobes and may promote the expansion of butyrate producers. Second, B100 ameliorates VPA-induced disturbances in lipid and amino acid metabolism, relieving metabolic stress on commensal microbes. Third, B100 decreases *Enterobacteriaceae*, a competitive pro-inflammatory Gram-negative family; this reduction may alleviate niche competition and facilitate the growth of beneficial butyrate-producing anaerobes. We note these findings are correlative, and further functional experiments are needed to clarify the causal relationship between MAO-A-mediated metabolic changes, gut microbiota reconstruction, and enrichment of butyrate-producing bacteria.

Importantly, recent mechanistic studies indicate that intestinal serotonergic homeostasis and host neurobehavioral regulation are modulated by multiple parallel pathways. Luminal aromatic amines, including phenethylamine and tyramine, can activate intestinal trace amine-associated receptor (TAAR) signaling in enterochromaffin cells, thereby directly regulating intestinal serotonin synthesis and host behavioral phenotypes. In the current study, we did not quantitatively detect the luminal concentrations of these aromatic amines, indicating that the observed behavioral and metabolic improvements cannot be exclusively attributed to MAO-A-mediated serotonin degradation. Changes in phenethylamine and tyramine levels and subsequent TAAR-dependent signaling may also contribute to these effects. Consequently, MAO-A-dependent modulation of serotonergic metabolism is one plausible but not definitive mechanism underlying the therapeutic effects of B100.

Consistent with prior investigations, our study provides further evidence that modulation of the gut microbiota and host metabolism can effectively alleviate ASD-related behavioral deficits. Multiple human studies have reported gut dysbiosis, altered tryptophan-serotonin metabolism, and perturbed lipid and amino acid profiles in subsets of ASD patients. These findings partly overlap with the microbial and

metabolic signatures identified in our VPA mouse model[7,24]. Unlike conventional probiotics with vague regulatory mechanisms, the engineered B100 strain combines a defined enzymatic function with effects on microbial composition and host metabolism and may therefore be suitable for ASD patients with gut dysbiosis and tryptophan/serotonin metabolic abnormalities. Although some microbiome and metabolic features overlap between human ASD and the VPA mouse model, we acknowledge important interspecies differences. In addition, we did not directly measure circulating inflammatory markers in the current study. Further clinical studies are required to validate these candidate biomarkers and evaluate the safety and efficacy of engineered probiotic intervention in human ASD populations.

Limitations

There are several limitations in this study that need to be considered. Firstly, although the VPA-induced mouse model is widely used in ASD research, it cannot recapitulate the full genetic and clinical heterogeneity of human ASD. B100 acts locally in the gut through MAO-A to regulate monoamine and amino acid metabolism. We expect B100 to benefit ASD models characterized by gut serotonin or tryptophan dysregulation and microbial dysbiosis. In contrast, its efficacy may be limited in models dominated by intrinsic neuronal or genetic defects without obvious peripheral metabolic disturbances. Future validation using genetic ASD models, including Shank3 and Cntnap2, is needed. Moreover, B100 was administered before ASD-related behaviors were fully established, restricting our conclusions to its preventive effects. While B100 may still modulate gut microbiota and metabolism after behavioral phenotypes emerge, established neurodevelopmental impairments may not respond to gut probiotic intervention. Further studies using therapeutic dosing are required to test whether B100 can reverse established ASD-related behaviors. Second, the correlative nature of our multi-omics data does not establish causality. Future mechanistic studies (fecal microbiota transplantation (FMT), antibiotic depletion or vagotomy) are needed to investigate the proposed gut-brain axis pathway. Third, because intestinal luminal aromatic amines (phenethylamine and tyramine) were not quantified, we cannot exclude a contribution from TAAR-mediated serotonergic regulation, limiting the mechanistic conclusions that can be drawn from the current work. Moreover, the clinical translation of B100 will require rigorous evaluation of long-term safety, particularly regarding plasmid retention, horizontal gene transfer, and potential off-target effects.

Conclusion

In summary, our findings indicate that the engineered probiotic expressing MAO-A could effectively alleviate ASD-related behaviors in a VPA-induced mouse model through coordinated modulation of the gut microbiota and systemic metabolism, accompanied by improvements in ASD-related behaviors. Our findings provide a foundation for developing precision microbial therapeutics for ASD and other neuropsychiatric disorders by targeting dysfunction of the gut-brain axis.

DECLARATIONS

Acknowledgements

The Graphical Abstract was created with BioRender.

Authors' contributions

Conducted the experiments: Hao C, Wen J, Wang J
Analyzed the data: Hao C, Wen J, Li X
Made a major contribution to writing the manuscript: Hao C
Reviewed the draft: Li Z, Hou W
supervised the research: Li Z, Hou W
Provided funding: Hou W
All authors have read the final manuscript and approved it for publication.

Availability of data and materials

All data supporting the findings of this study are provided in the article; additional information is available

from the corresponding authors upon reasonable request.

AI and AI-assisted tools statement

Not applicable.

Financial support and sponsorship

This work was supported by the Shanghai Magnolia Talent Plan Pujiang Project (24PJD135).

Conflicts of interest

The authors have declared no competing interests.

Ethics approval and consent to participate

The study protocol was approved by the Institutional Animal Care and Use Committee of Shanghai Tenth People's Hospital (SHDSYY-2021-4977).

Consent for publication

Not applicable.

Copyright

© The Author(s) 2026.

REFERENCES

1. Abrahams BS, Geschwind DH. Advances in autism genetics: on the threshold of a new neurobiology. *Nat Rev Genet.* 2008;9:341-55. DOI PubMed PMC
2. Maenner MJ, Warren Z, Williams AR, et al. Prevalence and characteristics of autism spectrum disorder among children aged 8 years - autism and developmental disabilities monitoring network, 11 sites, United States, 2020. *MMWR Surveill Summ.* 2023;72:1-14. DOI PubMed PMC
3. Hsiao EY, McBride SW, Hsien S, et al. Microbiota modulate behavioral and physiological abnormalities associated with neurodevelopmental disorders. *Cell.* 2013;155:1451-63. DOI PubMed PMC
4. Chernikova MA, Flores GD, Kilroy E, Labus JS, Mayer EA, Aziz-Zadeh L. The Brain-gut-microbiome system: pathways and implications for autism spectrum disorder. *Nutrients.* 2021;13:4497. DOI PubMed PMC
5. Cryan JF, O'Riordan KJ, Cowan CSM, et al. The microbiota-gut-brain axis. *Physiol Rev.* 2019;99:1877-2013. DOI
6. Wu J, Yang Y, Li T, et al. Genome-integrated engineering of *Escherichia coli* Nissle 1917 enables sustained gut-local biosynthesis of 5-hydroxytryptophan. *Synth Syst Biotechnol.* 2027;18:13-24. DOI PubMed PMC
7. Bu W, Chen Z, Liu B, Jia X. Gut microbiota and its metabolism in autism spectrum disorder: from pathogenesis to therapy. *Front Cell Infect Microbiol.* 2025;15:1687691. DOI PubMed PMC
8. Spohn SN, Mawe GM. Non-conventional features of peripheral serotonin signalling - the gut and beyond. *Nat Rev Gastroenterol Hepatol.* 2017;14:412-20. DOI PubMed PMC
9. Israelyan N, Margolis KG. Serotonin as a link between the gut-brain-microbiome axis in autism spectrum disorders. *Pharmacol Res.* 2018;132:1-6. DOI PubMed PMC
10. Wong AC, Devason AS, Umana IC, et al. Serotonin reduction in post-acute sequelae of viral infection. *Cell.* 2023;186:4851-4867.e20. DOI
11. Akram N, Faisal Z, Irfan R, et al. Exploring the serotonin-probiotics-gut health axis: A review of current evidence and potential mechanisms. *Food Sci Nutr.* 2024;12:694-706. DOI PubMed PMC
12. Zhang Z, Kang W, Mi Y, Zhong X, He Y. The microbiota-gut-brain axis in autism: associations, causal inference, and interventions - a narrative review. *Pathogens.* 2025;14:1145. DOI PubMed PMC
13. Shen J, Gao J, Gao L, et al. Melatonin ameliorates autistic-like behaviors by restoring gut microbiota-derived tryptophan metabolites. *Cell Mol Life Sci.* 2026;83:154. DOI PubMed PMC
14. Sun X, Li N, Zhong P, Chen L, Sun J. Development of MAO-A and 5-HT_{2A}R dual inhibitors with improved antidepressant activity. *J Med Chem.* 2022;65:13385-400. DOI
15. Xu J, Lu Y. The microbiota-gut-brain axis and central nervous system diseases: from mechanisms of pathogenesis to therapeutic strategies. *Front Microbiol.* 2025;16:1583562. DOI PubMed PMC
16. Hu S, Fei M, Fu B, et al. Development of probiotic *E. coli* Nissle 1917 for β-alanine production by using protein and metabolic engineering. *Appl Microbiol Biotechnol.* 2023;107:2277-88. DOI

17. Nicolini C, Fahnestock M. The valproic acid-induced rodent model of autism. *Exp Neurol.* 2018;299:217-27. DOI PubMed
18. Wu HF, Chen YJ, Chu MC, et al. Deep brain stimulation modified autism-like deficits via the serotonin system in a valproic acid-induced rat model. *Int J Mol Sci.* 2018;19:2840. DOI PubMed PMC
19. Zhang B, Wang L, Zhan A, et al. Long-term exposure to a hypomagnetic field attenuates adult hippocampal neurogenesis and cognition. *Nat Commun.* 2021;12:1174. DOI PubMed PMC
20. Tong M, Jacobs JP, McHardy IH, Braun J. Sampling of intestinal microbiota and targeted amplification of bacterial 16S rRNA genes for microbial ecologic analysis. *Curr Protoc Immunol.* 2014;107:7.41.1-7.41.11. DOI PubMed PMC
21. Edgar RC. UPARSE: highly accurate OTU sequences from microbial amplicon reads. *Nat Methods.* 2013;10:996-8. DOI PubMed
22. Jiménez-Pareyón GR, Cristóbal-Luna JM, García-Martínez Y, et al. Psychobiotics at the frontiers of neurodegenerative and neuropsychiatric research. *Microorganisms.* 2025;13:2718. DOI PubMed PMC
23. Li H, Niu R, He W, et al. *Lachnospira eligens* attenuates epileptogenesis via gut-brain axis regulation of blood-brain barrier integrity and neuroinflammation. *Theranostics.* 2026;16:1045-62. DOI PubMed PMC
24. Petropoulos A, Stavropoulou E, Tsigalou C, Bezirtzoglou E. Microbiota gut-brain axis and autism spectrum disorder: mechanisms and therapeutic perspectives. *Nutrients.* 2025;17:2984. DOI PubMed PMC

Disclaimer/Publisher's Note: All statements, opinions, and data contained in this publication are solely those of the individual author(s) and contributor(s) and do not necessarily reflect those of OAE and/or the editor(s). OAE and/or the editor(s) disclaim any responsibility for harm to persons or property resulting from the use of any ideas, methods, instructions, or products mentioned in the content.

© The Author(s) 2026. Open Access This article is licensed under a Creative Commons Attribution 4.0 International License (https://creativecommons.org/licenses/by/4.0/), which permits unrestricted use, sharing, adaptation, distribution and reproduction in any medium or format, for any purpose, even commercially, as long as you give appropriate credit to the original author(s) and the source, provide a link to the Creative Commons license, and indicate if changes were made.